ADVANCED FUNCTIONAL MATERIALS

Supporting Information

for *Adv. Funct. Mater.,* DOI: 10.1002/adfm.202204794

Carbon Nanotube Array-Based Flexible Multifunctional Electrodes to Record Electrophysiology and Ions on the Cerebral Cortex in Real Time

Han Yang, Zheyan Qian, Jiajia Wang, Jianyou Feng, Chengqiang Tang, Liyuan Wang, Yue Guo, Ziwei Liu, Yiqing Yang, Kailin Zhang, Peining Chen, Xuemei Sun, and Huisheng Peng**

Supporting Information

Carbon Nanotube Array-based Flexible Multifunctional Electrodes to Record Electrophysiology and Ions on the Cerebral Cortex in Real Time

Han Yang, Zheyan Qian, Jiajia Wang, Jianyou Feng, Chengqiang Tang, Liyuan Wang, Yue Guo, Ziwei Liu, Yiqing Yang, Kailin Zhang, Peining Chen, Xuemei Sun and Huisheng Peng**

H. Yang, Z. Qian, J. Wang, J. Feng, C. Tang, Dr. L. Wang, Y. Guo, Z. Liu, Y. Yang, K. Zhang, Prof. P. Chen, Prof. X. Sun, Prof. H. Peng
State Key Laboratory of Molecular Engineering of Polymers, Department of Macromolecular Science and Laboratory of Advanced Materials, Fudan University, Shanghai 200438, China, E-mail: sunxm@fudan.edu.cn; penghs@fudan.edu.cn.

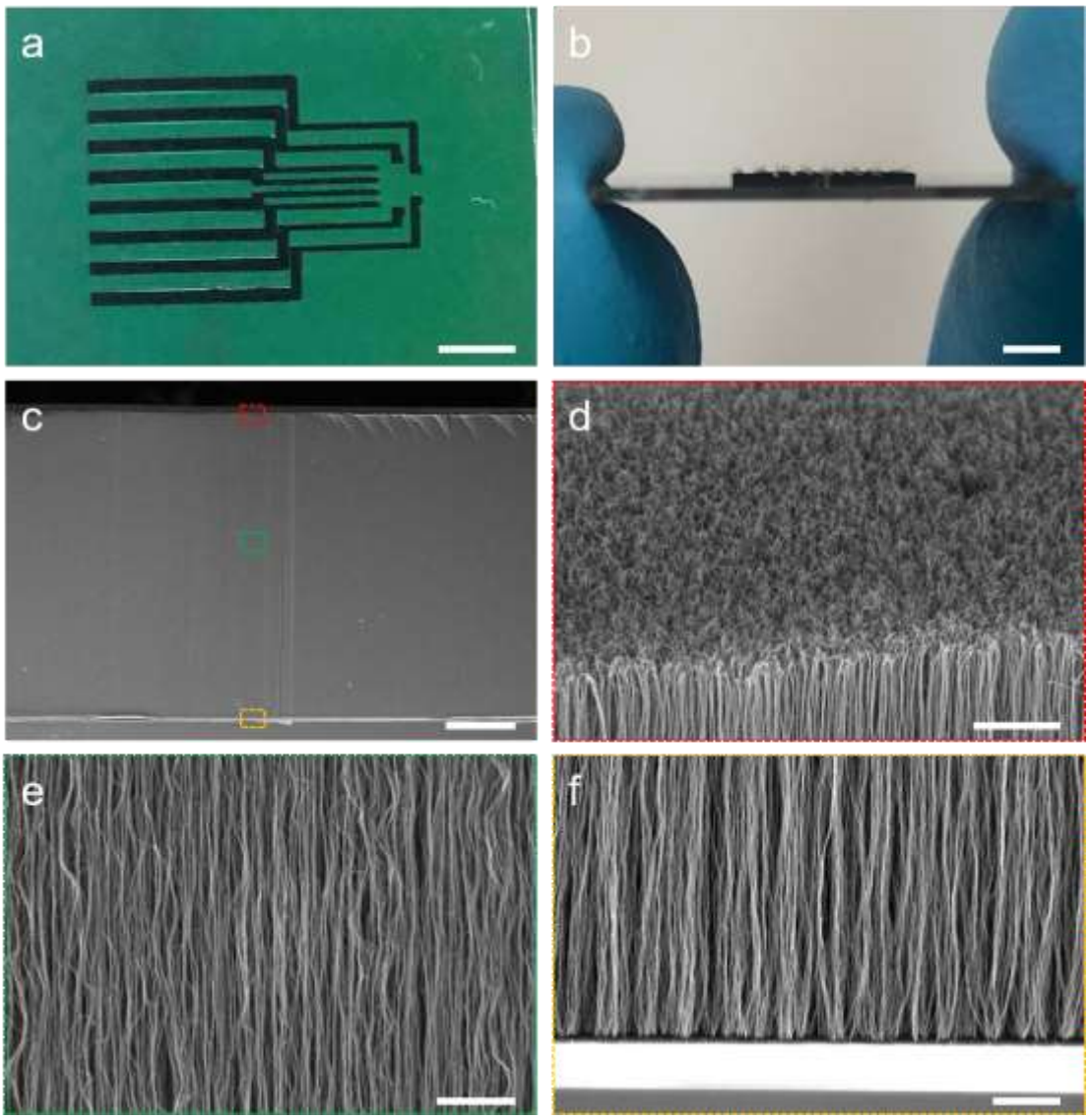

Figure S1. Morphological characterization of vertically aligned CNTA on the silicon wafer. a) Photograph of CNTA from top view. b) Photograph of CNTA from side view. Scale bar: 5 mm. c) SEM image of CNTA from side view. Scale bar: 100 μm. d) Enlarged SEM image of the top of CNTA as marked with red dotted box in (c). Scale bar: 2 μm. e) Enlarged SEM image of the middle of CNTA as marked with green dotted box in (c). Scale bar: 2 μm. f) Enlarged SEM image of the bottom of CNTA as marked with yellow dotted box in (c). Scale bar: 1 μm.

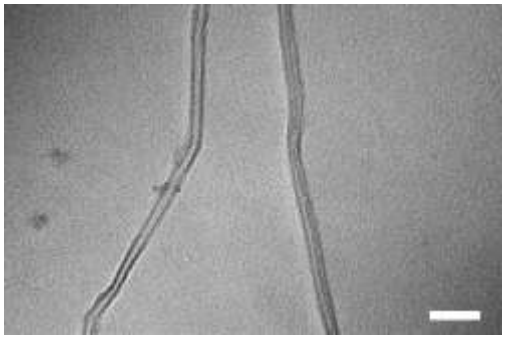

Figure S2. Transmission electron microscopy image of carbon nanotubes. Scale bar: 50 nm.

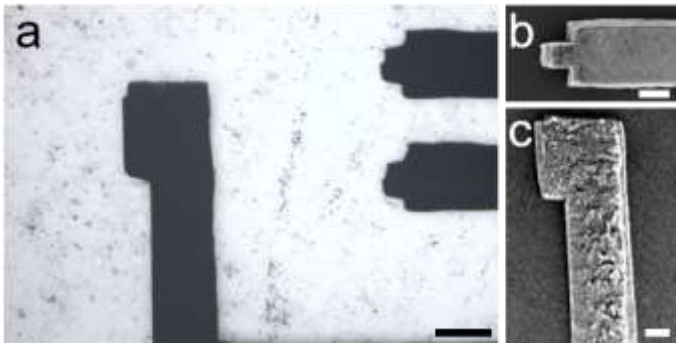

Figure S3. a) Photograph of the flexible CNTA electrodes. b) SEM image of the site for ECoG recording. c) SEM image of the site for the ion-selective electrode. Scale bar: 200 μm (a), 100 μm (b), 100 μm (c).

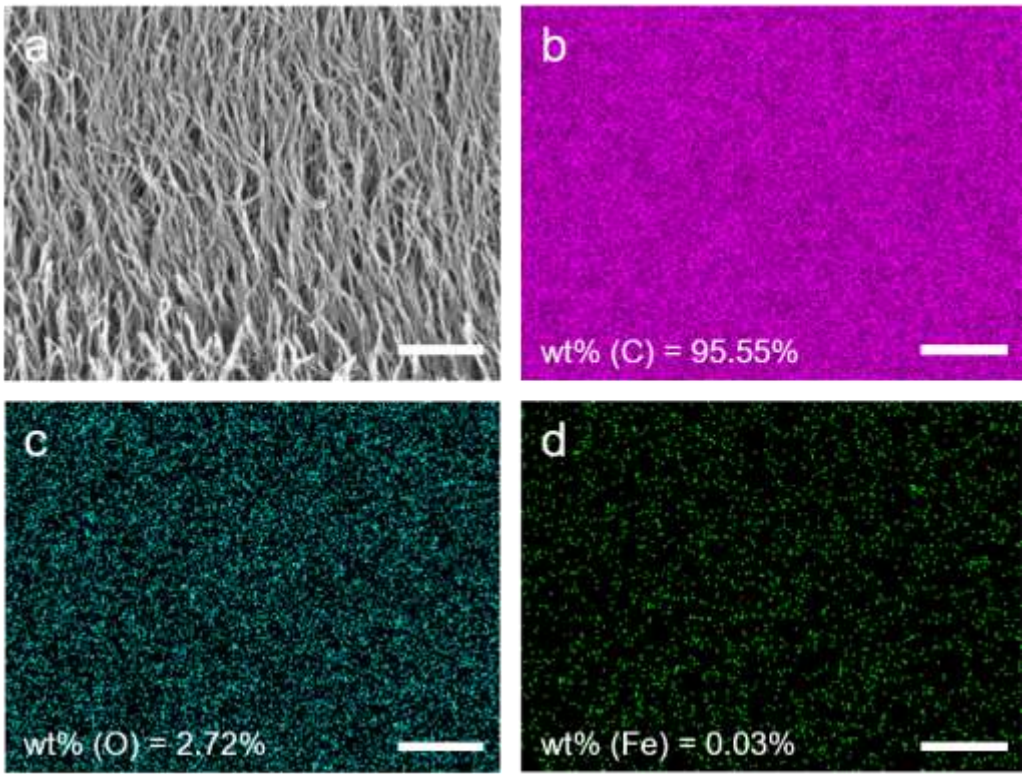

Figure S4. a) SEM image of CNTA transferred by PDMS film. b-d) Energy dispersive spectra elemental mapping images of C (b), O (c) and Fe (d). Scale bar: 1 µm.

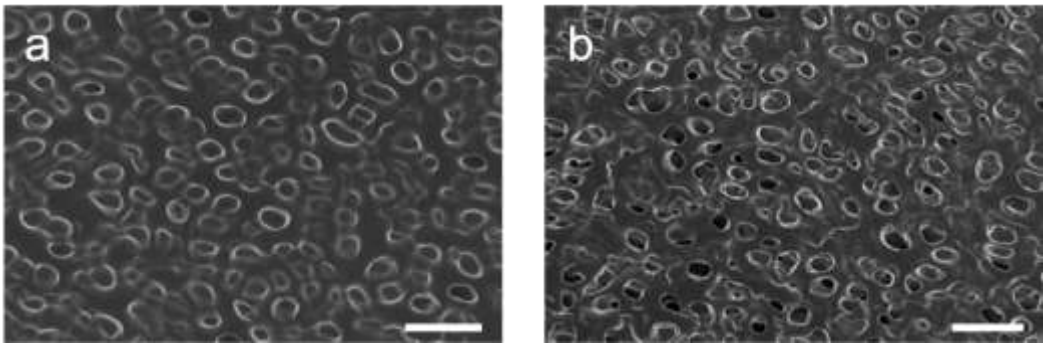

Figure S5. SEM images of ion-selective membranes. a) K^+ selective membrane. b) Na^+ selective membrane. Scale bar: 10 μm.

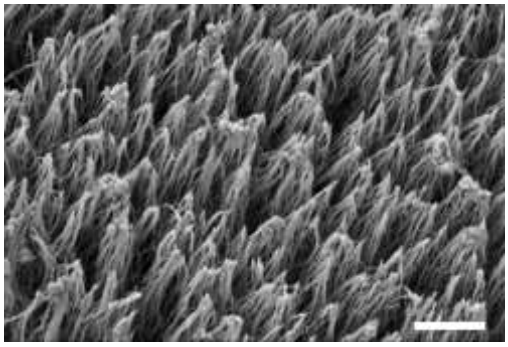

Figure S6. SEM image of CNTA-based Ag/AgCl electrode prepared by electroplating. Scale bar: 2 μm.

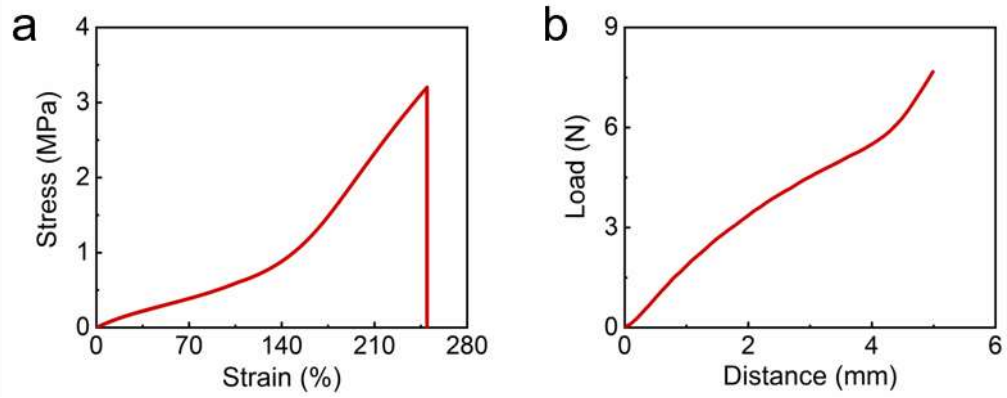

Figure S7. Mechanical properties of PDMS film. a) Tensile stress-strain curve. b) Bending curve.

Figure S8. Photograph of FME attached to a rat brain model prepared from 0.6 wt% agar. The yellow arrow points to the location of FME. Scale bar: 1 cm.

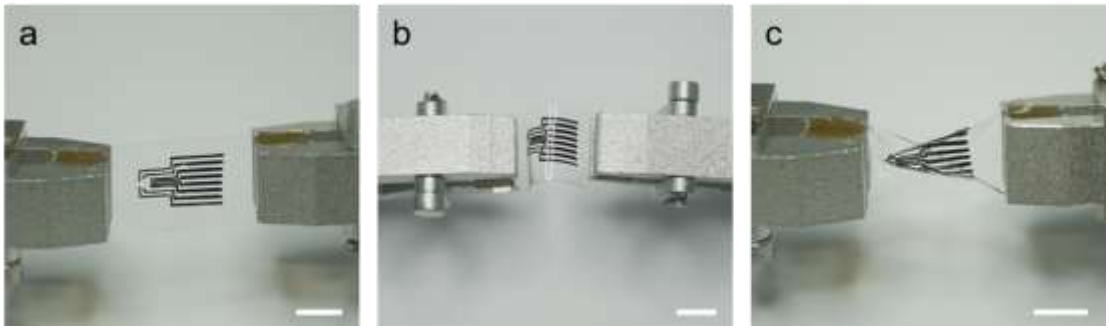

Figure S9. Photographs of FME under different states. a) Tension. b) Bending. c) Torsion. Scale bar: 1cm.

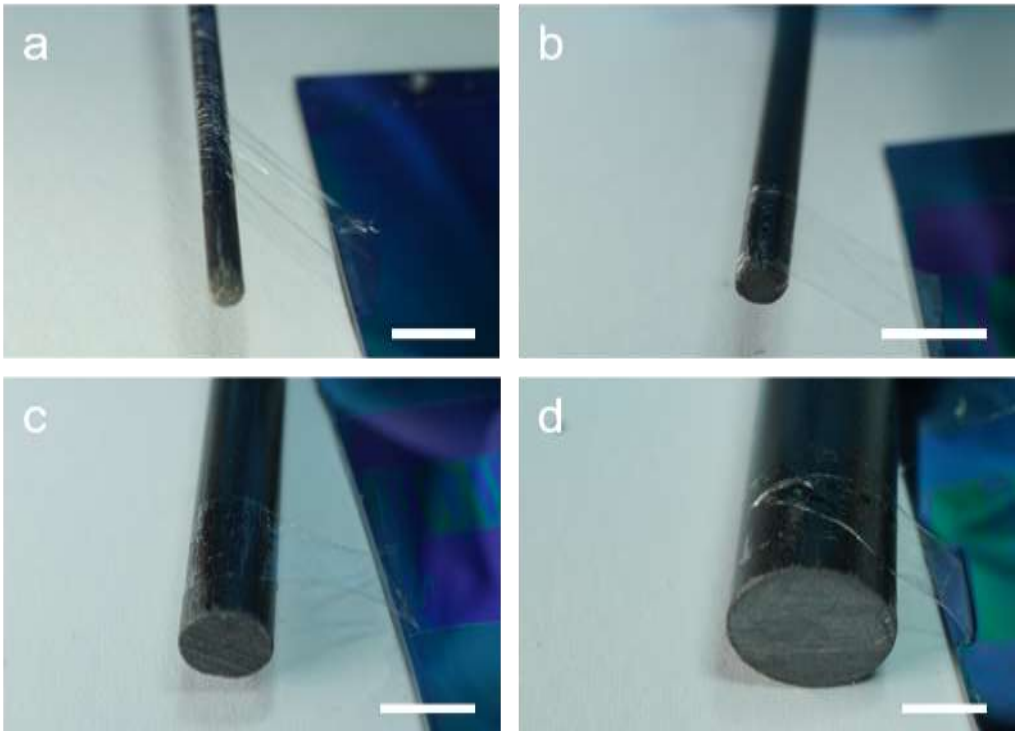

Figure S10. Photographs of thin PDMS film (about 1 μm in thickness) wound on cylinders with different radius of curvature. a) 0.2 cm. Scale bar: 0.5 cm. b) 0.5 cm. Scale bar: 1 cm. c) 1 cm. Scale bar: 1 cm. d) 2 cm. Scale bar: 1 cm.

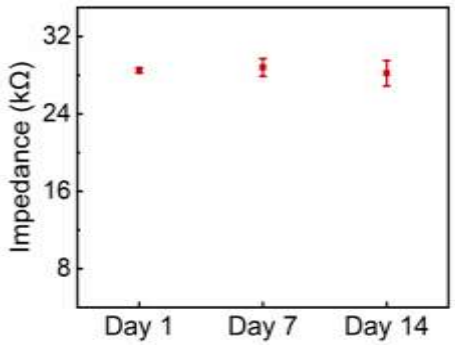

Figure S11. Impedance stability of CNTA electrodes in artificial cerebrospinal fluid (aCSF) at 37 °C. All values represent means ± standard deviations (n = 3).

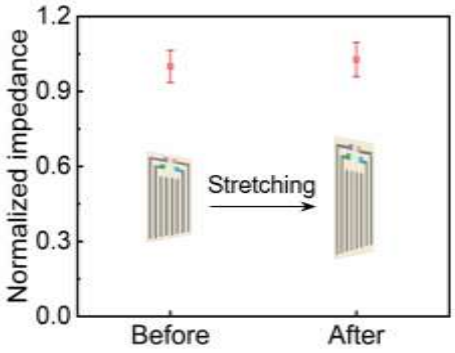

Figure S12. Changes in impedance of ECoG electrodes before and after 1,000 stretching cycles with a strain of 10%. All values represent means ± standard deviations (n = 3).

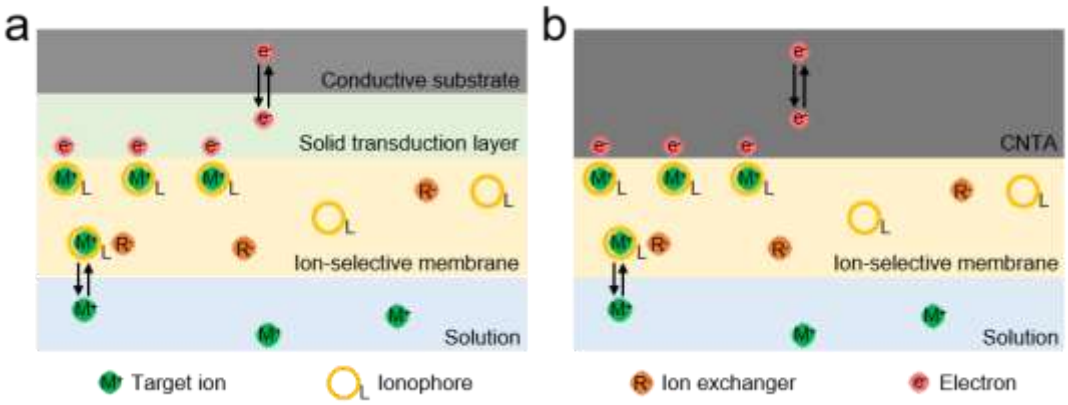

Figure S13. a) Schematic diagram of the sensing mechanism of the conventional ion-selective electrode. b) Schematic diagram of CNTA-based ion-selective electrode with CNTA served as both conductive substrate and transduction layer.

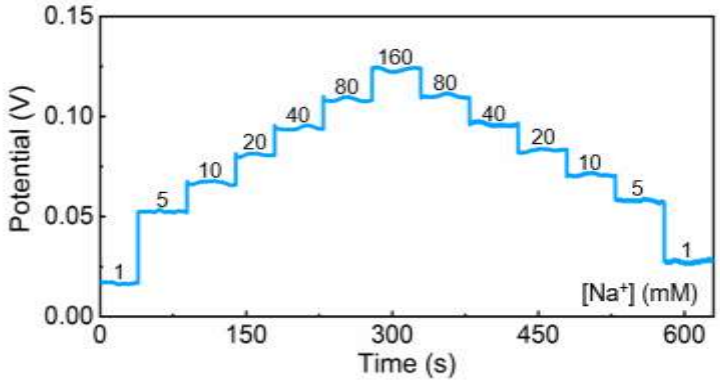

Figure S14. Repeatability of Na^+ selective electrode.

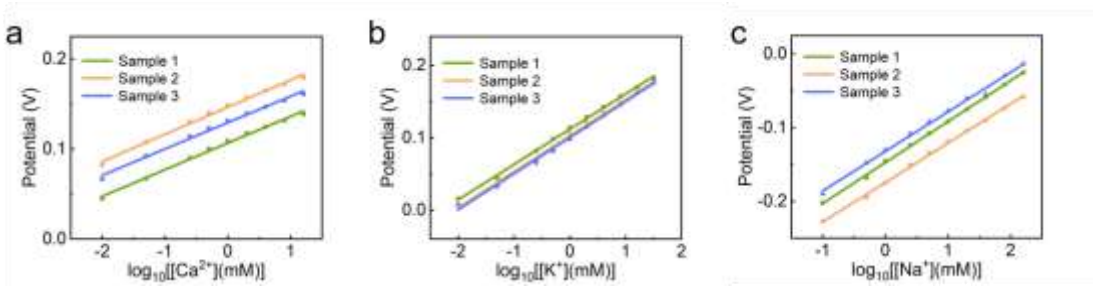

Figure S15. Reproducibility of ion-selective electrodes. a) Ca^{2+} selective electrode. b) K^{+} selective electrode. c) Na^{+} selective electrode. The three colors represent three different samples for each kind of sensor.

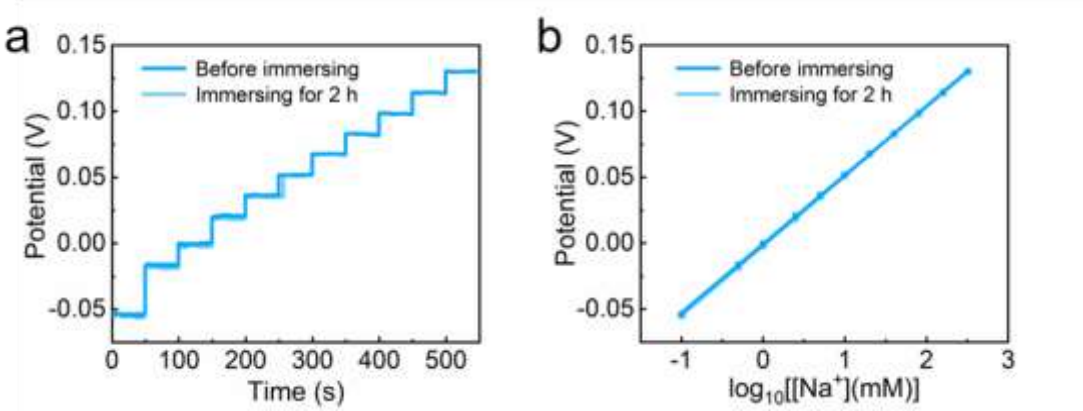

Figure S16. The sensing performances of Na^+ selective electrode before and after being immersed in aCSF containing 40 mg/mL BSA. a) The open-circuit potential response. b) The sensitivity fitting curves.

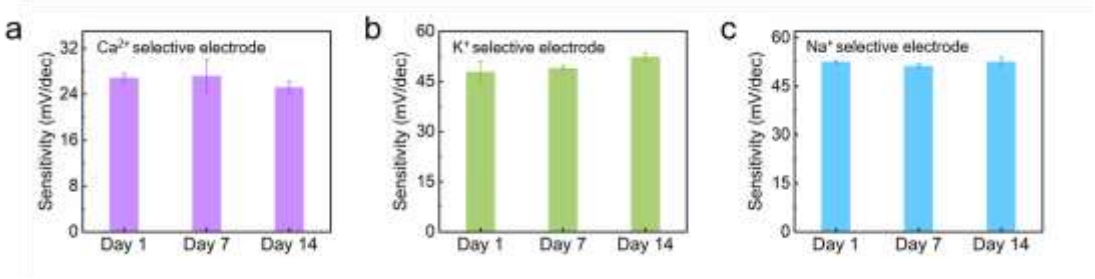

Figure S17. Long-term stability of ion-selective electrodes immersed in aCSF at 37 °C. All values represent means ± standard deviations (n = 3).

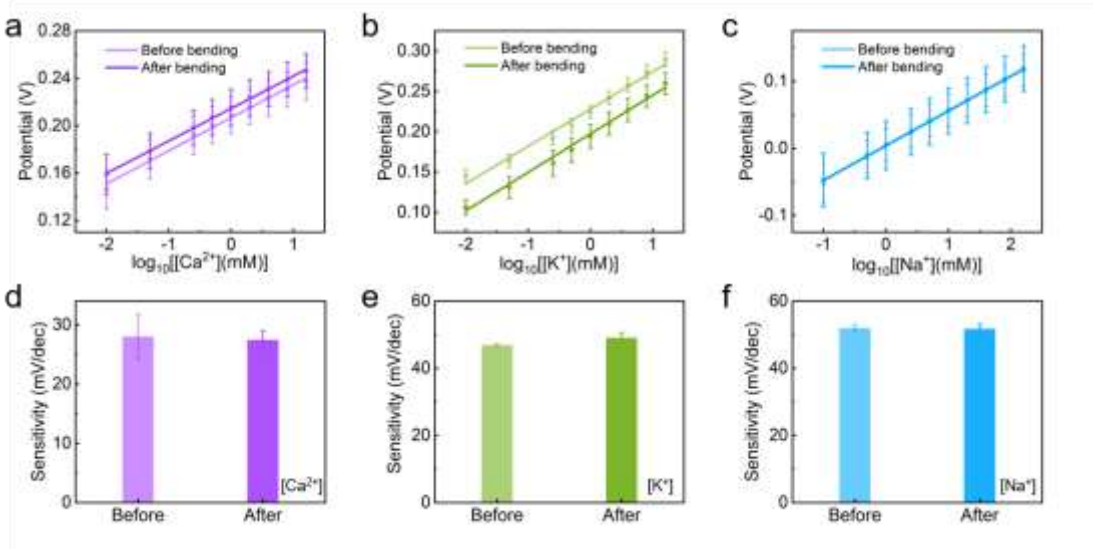

Figure S18. Dynamic stability of ion-selective electrodes. a-c) Sensitivity fitting curves of Ca^{2+} (a), K^+ (b) and Na^+ (c) selective electrodes before and after 10,000 bending cycles with a bending radius of 7 mm. All values represent means ± standard deviations (n = 3). d-f) Sensitivity comparison of Ca^{2+} (a), K^+ (b) and Na^+ (c) selective electrodes to corresponding ions before and after 10,000 bending cycles. All values represent means ± standard deviations (n = 3).

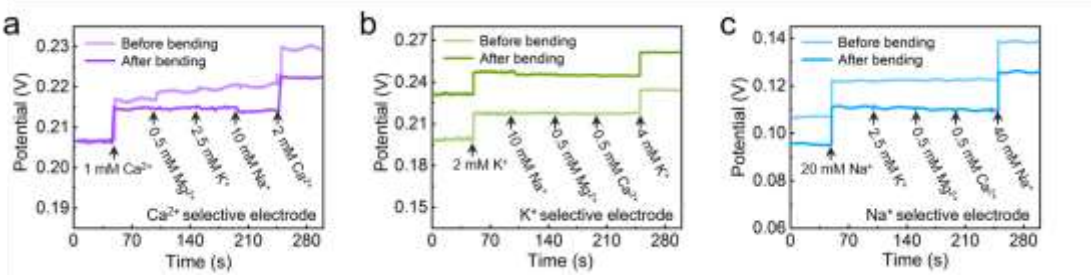

Figure S19. Selectivity of ion-selective electrodes before and after 10,000 bending cycles with a bending radius of 7 mm. a) Ca^{2+} selective electrode. b) K^{+} selective electrode. c) Na^{+} selective electrode. The base solutions are 1 mM $CaCl_2$, 2 mM KCl and 20 mM NaCl, respectively.

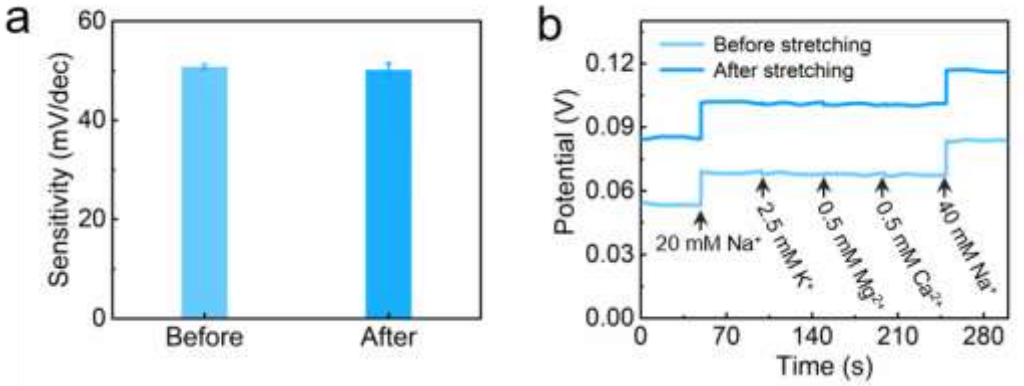

Figure S20. The performances of Na^+ selective electrodes before and after 1,000 stretching cycles with a strain of 10%. a) Sensitivity. All values represent means ± standard deviations (n = 3). b) Selectivity. The base solution is 20 mM NaCl.

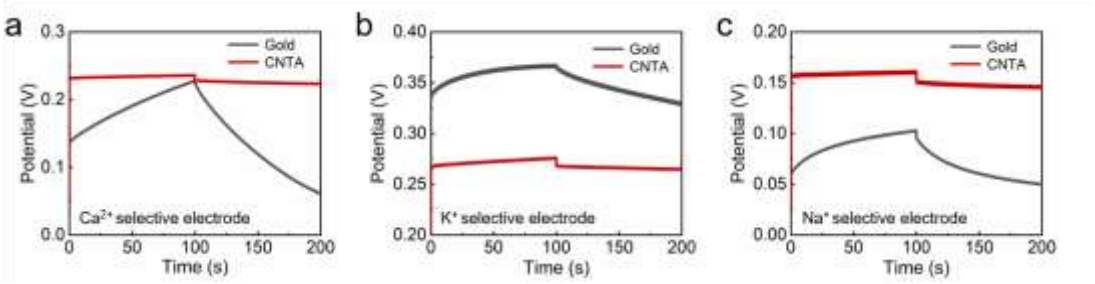

Figure S21. Chronopotentiograms of ion-selective electrodes with CNTA and gold as conductive substrates. a) Ca^{2+} selective electrode. b) K^{+} selective electrode. c) Na^{+} selective electrode. 1 nA and -1 nA were applied for the former and the latter 100 s, respectively.

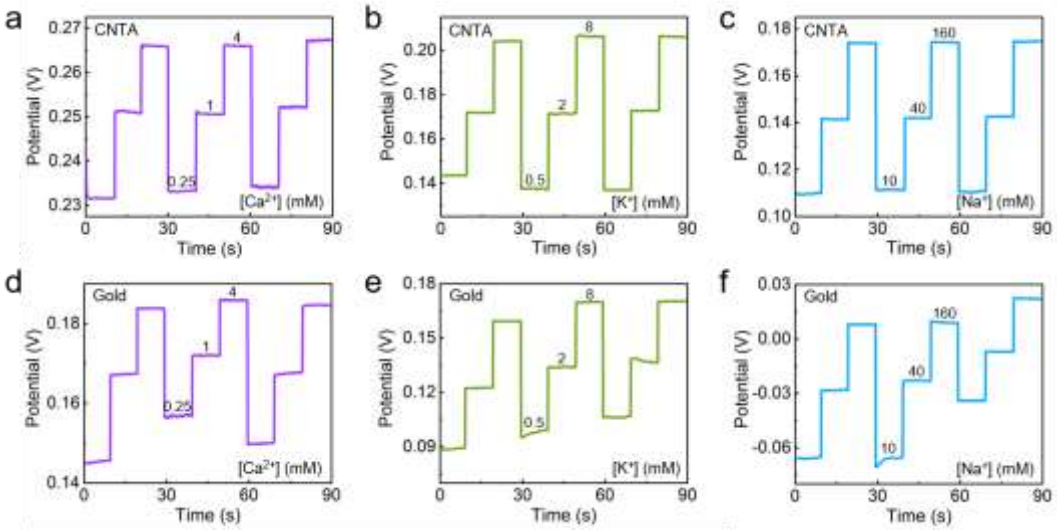

Figure S22. a-c) Reversible responses of Ca^{2+} (a), K^+ (b) and Na^+ (c) selective electrodes to corresponding ions with CNTA as a conductive substrate. d-f) Reversible responses of Ca^{2+} (d), K^+ (e) and Na^+ (f) selective electrodes to corresponding ions with gold as a conductive substrate.

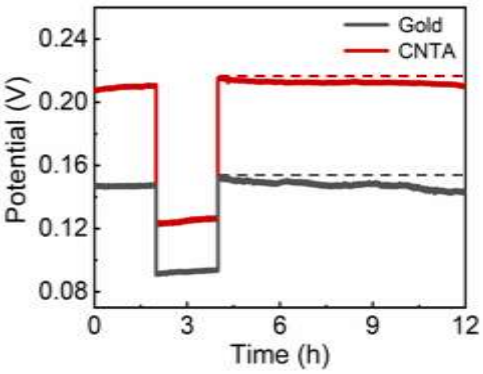

Figure S23. Water layer test for the CNTA-based and gold-based Ca^{2+} selective electrodes. The Ca^{2+} selective electrodes were sequentially immersed in 1 mM $CaCl_2$ for 2 h, 1 mM $MgCl_2$ for 2 h and 1 mM $CaCl_2$ for 8 h. The potential drift was the difference between the dotted line and the corresponding recording curve at 12 h.

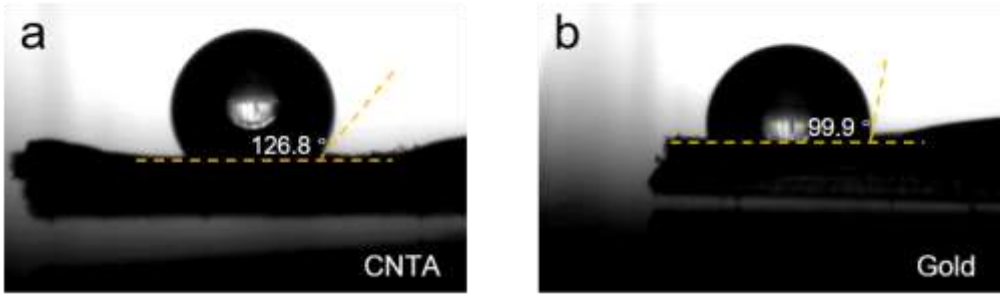

Figure S24. Water contact angles of different electrodes. a) CNTA. b) Gold.

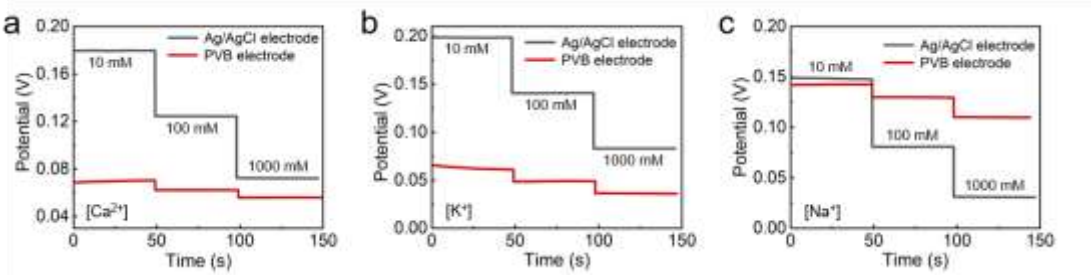

Figure S25. Potential responses of Ag/AgCl and PVB electrodes to different cations. a) Ca^{2+}. b) K^{+}. c) Na^{+}.

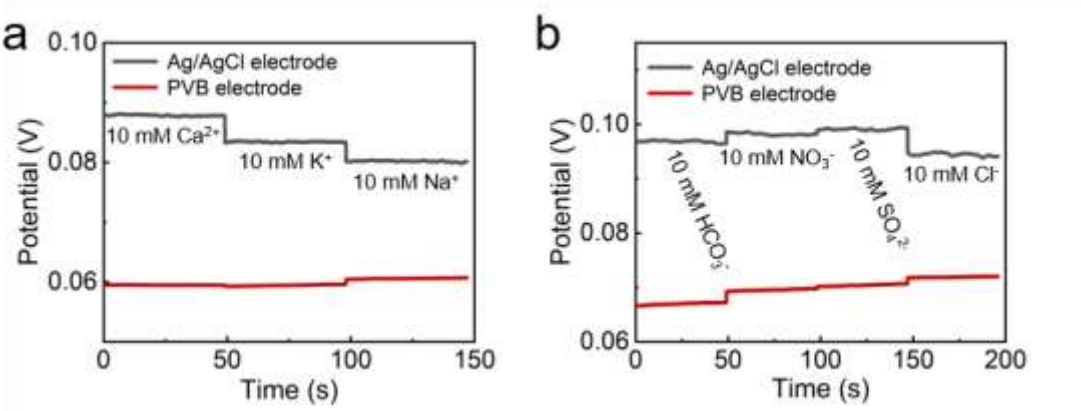

Figure S26. Potential responses of Ag/AgCl and PVB electrodes to different cations (a) and different anions (b). The base solution is 50 mM NaCl.

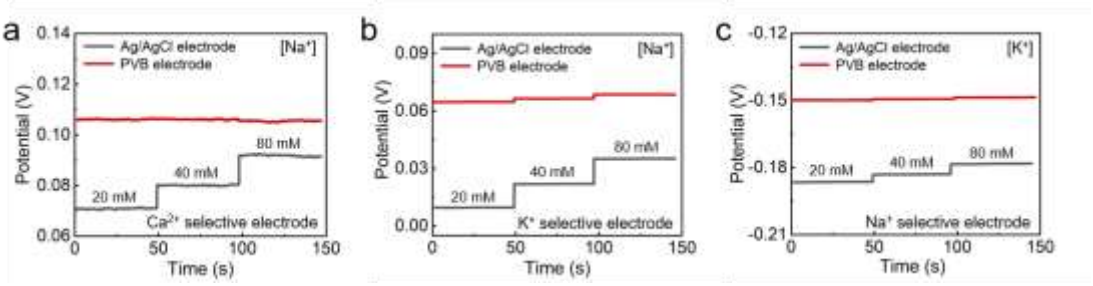

Figure S27. Anti-interference properties of ion-selective electrodes with Ag/AgCl and PVB electrodes as reference electrodes. a) Ca^{2+} selective electrode. b) K^{+} selective electrode. c) Na^{+} selective electrode.

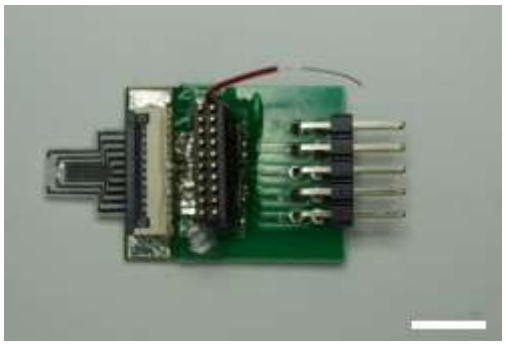

Figure S28. Photograph of FME connected to a circuit board. Scale bar: 1 cm.

Figure S29. Photograph of a rat with FME implanted on the cerebral cortex. Scale bar: 3 cm.

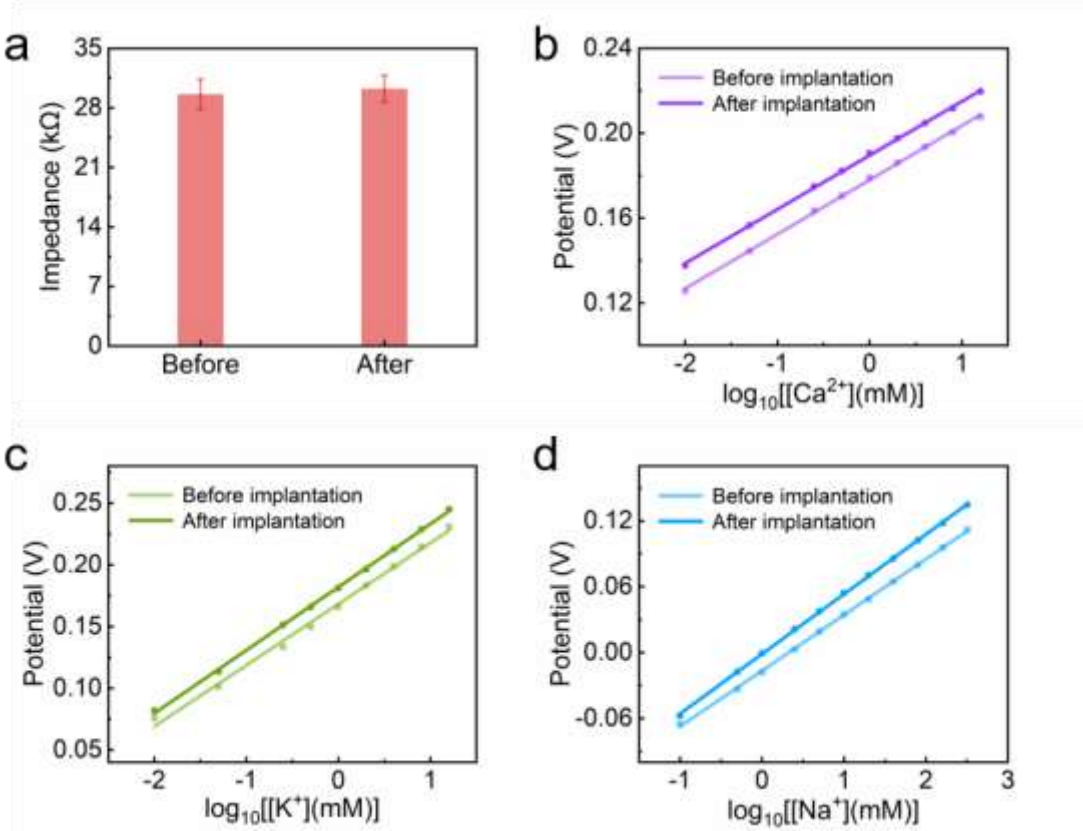

Figure S30. The performances of FME before and after implantation on the cerebral cortex for 4 h. a) The impedance of ECoG electrodes. b) Sensitivity fitting curves of Ca^{2+} selective electrodes. c) Sensitivity fitting curves of K^{+} selective electrodes. d) Sensitivity fitting curves of Na^{+} selective electrodes.

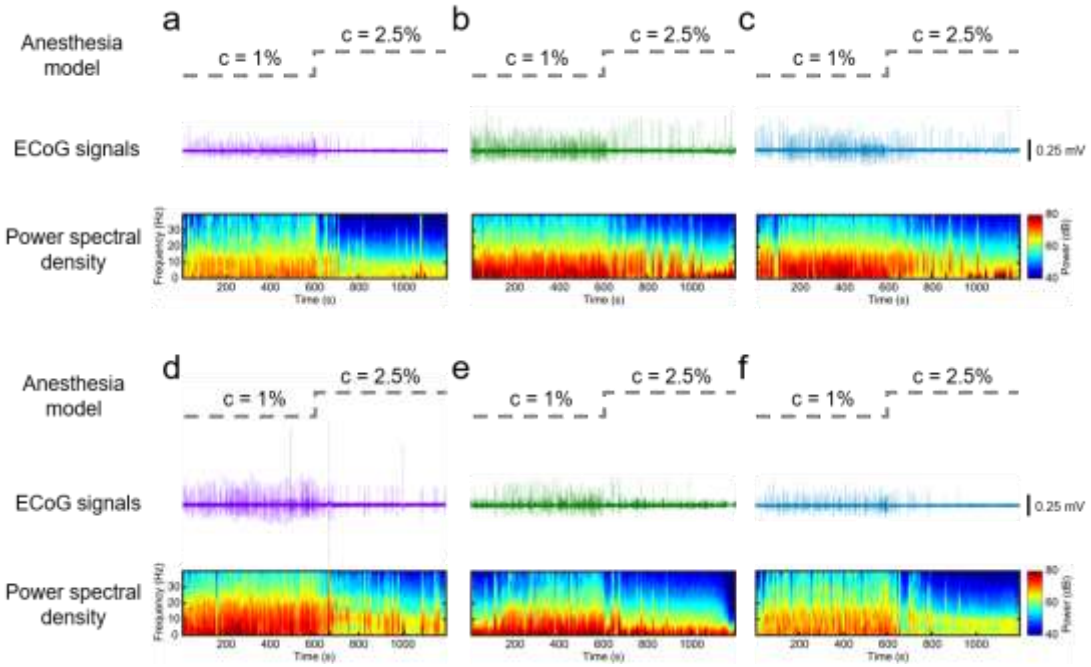

Figure S31. a-c) Changes in ECoG signals simultaneously recorded with different ions of Ca^{2+} (a), K^{+} (b) and Na^{+} (c) after implantation of FME for 1 week, respectively. Corresponding power spectral densities were further calculated. d-f) Changes in ECoG signals simultaneously recorded with different ions of Ca^{2+} (d), K^{+} (e) and Na^{+} (f) after implantation of FME for 2 weeks, respectively. Corresponding power spectral densities were further calculated.

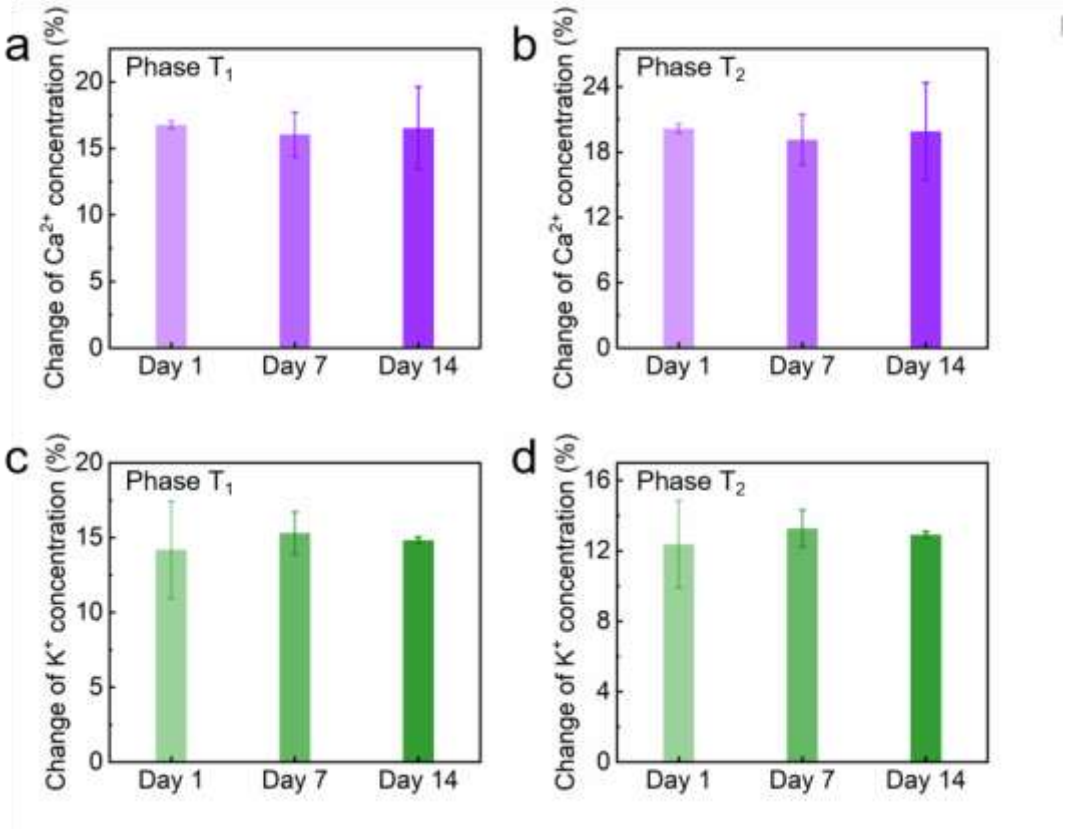

Figure S32. a, b) The change of Ca^{2+} concentration at phase T_1 (a) and T_2 (b) during 14 days. All values represent means ± standard deviations (n = 3). c, d) The change of K^+ concentration at phase T_1 (c) and T_2 (d) during 14 days. All values represent means ± standard deviations (n = 3).

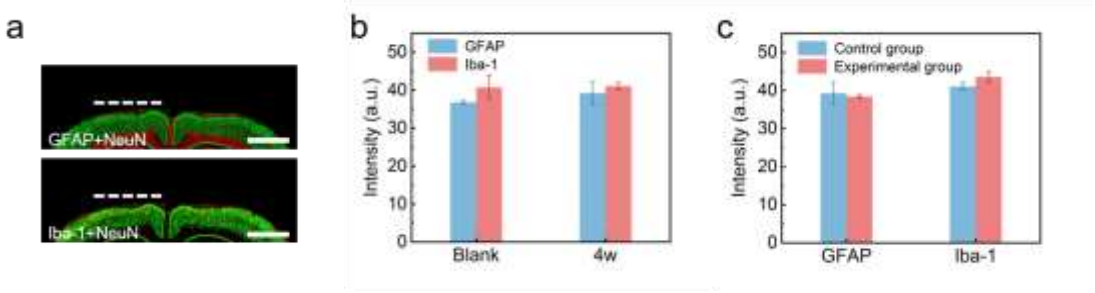

Figure S33. Biocompatibility characterization of FME implanted in the brain of rat for 4 weeks. a) Fluorescence images of coronal brain slices labeled with astrocytes (GFAP, red, top), microglia (Iba-1, red, bottom) and neurons (NeuN, green) (n = 3). The white dotted line indicates the position of FME. Scale bar: 2 mm. b) Averaged fluorescence intensities of GFAP and Iba-1 in the blank and control groups in 4 weeks after implantation. All values represent means ± standard deviations (n = 3). c) Averaged fluorescence intensities of GFAP and Iba-1 in the control and experimental groups in 4 weeks after implantation. All values represent means ± standard deviations (n = 3).